Chiral Porous Metal–Organic Frameworks of Co(II) and Ni(II): Synthesis, Structure, Magnetic Properties, and CO2 Uptake

ARTICLE *in* CRYSTAL GROWTH & DESIGN · JANUARY 2012

Impact Factor: 4.89 · DOI: 10.1021/cg201447c

4 AUTHORS, INCLUDING:

C. M. Nagaraja
Indian Institute of Technology Ropar
24 PUBLICATIONS **236** CITATIONS
SEE PROFILE

Ritesh Haldar
Jawaharlal Nehru Centre for Advanced Scienti…
27 PUBLICATIONS **360** CITATIONS
SEE PROFILE

Tapas Maji
Jawaharlal Nehru Centre for Advanced Scienti…
176 PUBLICATIONS **4,297** CITATIONS
SEE PROFILE

CRYSTAL GROWTH & DESIGN

Article

pubs.acs.org/crystal

Chiral Porous Metal−Organic Frameworks of Co(II) and Ni(II): Synthesis, Structure, Magnetic Properties, and CO_2 Uptake

C. M. Nagaraja,[†] Ritesh Haldar,[‡] Tapas Kumar Maji,*[,†,‡] and C. N. R. Rao*[,†,‡]

[†]Chemistry and Physics of Materials Unit and [‡]New Chemistry Unit, Jawaharlal Nehru Center for Advanced Scientific Research, Jakkur, Bangalore, 560064, India

Supporting Information

ABSTRACT: Four isostructural chiral three-dimensional (3D) porous pillared-layer frameworks based on Co(II) and Ni(II), $\{[M(L\text{-mal})(azpy)_{0.5}]\cdot 2H_2O\}_n$ (M = Co (**1**), Ni (**2**)) and $\{[M(L\text{-mal})(bpee)_{0.5}]\cdot H_2O\}_n$(M = Co (**3**), Ni (**4**)); (L-mal = L-malate dianion, azpy = 4,4′-bisazobipyridine, and bpee = 1,2-bis(4-pyridyl)ethylene), have been synthesized using mixed ligand systems and characterized structurally. All the frameworks are homochiral, based on the chiral L-malate dianion. The bridging of L-malate with Co(II) or Ni(II) forms a two-dimensional (2D) layer of $\{M(L\text{-mal})\}_n$ which is further pillared by azpy or bpee to form a 3D pillared-layer porous framework. The large rectangular channels along the crystallographic *b* direction (7.0 × 6.2 Å^2 for **1** and **2**; 6.8 × 6.1 Å^2 for **3** and **4**) are occupied by the guest water molecules. The binding of −OH and −COO groups of L-malate with the Co(II) or Ni(II) render interesting antiferromagnetic and ferrimagnetic type behavior in **1** and **2**, respectively. All the frameworks show high thermal stability and guest-induced structural contraction evidenced by the temperature-dependent powder X-ray diffraction patterns. Gas (N_2, CO_2, H_2, O_2, and Ar) adsorption studies on the dehydrated frameworks of **1** and **3** show excellent selective CO_2 gas uptake at 195 K. The lesser uptake of CO_2 in the dehydrated framework of **3** compared to **1** has been rationalized to the different polarity of the pore surface due to the change in the functional group of the pillar module. The more polar azo (−N═N−) group in **1** renders strong interaction with CO_2 compared to the ethylenic (−CH═CH−) group in **3**. The difference in polarity in **1** and **3** also is reflected in water sorption studies.

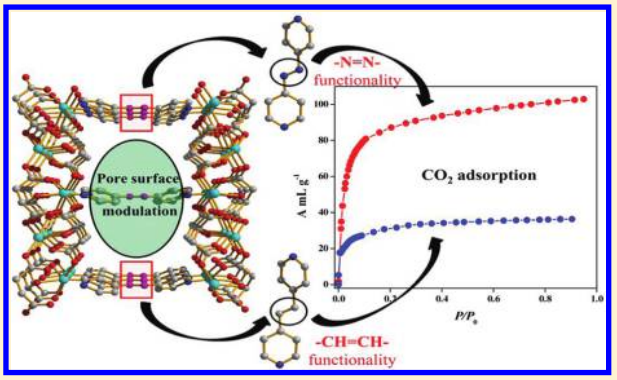

INTRODUCTION

There is an upsurge in research on functional porous coordination polymers (PCPs) or metal−organic frameworks (MOFs) obtained by connecting the metal ions or clusters (SBU) with a variety of organic spacers in recent years.[1−4] Possessing the merits of both organic and inorganic building units, MOFs have outperformed other contemporary porous materials such as zeolites and activated carbons.[5−7] The porous nature and tunable and regular-shaped channels make MOFs useful materials for gas storage, catalysis,[8−11] separation,[12−15] and drug delivery[16,17] applications. Synthesis and functionalization to make a multipurpose MOF material, that is, to impose versatile functionalities in the framework are major challenges in generating such novel materials. A review of the recent progress in this direction shows that there are very few examples of such materials. Imposing chirality, magnetism, and porosity in the same material has not been altogether successful.[18,19]

It is to be noted that the occurrence of porosity and magnetism in the same material is not common. Magnetism works over short distances, while porosity develops from long organic linkers. Coexistence of these two contrary properties is possible by a judicious choice of linkers and metal ions. Incorporation of magnetic moment carriers such as paramagnetic metal ions helps to impart magnetic properties, but this alone is not enough as magnetism being a cooperative phenomenon requires connectivity between moment carriers.[20] This brings up the critical role of organic spacers in these hybrid materials. Organic spacers with different coordination sites (like OH^-, COO^-) can endow structural diversity. An analysis of documented frameworks with such linkers reveals the potential of constructing magnetic coordination polymers, which can effectively mediate magnetic coupling between the metal centers to different degrees.[21−26] The malate anion is promising in this context as it connects a number of metal ions through variety of possible coordination modes (bidentate, tridentate, tetradentate, and pentadentate)[27−30] and can effectively mediate ferromagnetic, antiferromagnetic, or ferrimagnetic[31,32] coupling between the metal centers. The presence of a hydroxyl group gives an additional coordination site and allows the formation of five- and six-membered rings which provide extra stability to the framework.[33−35] Moreover,

Received: November 1, 2011
Revised: December 22, 2011
Published: January 3, 2012

   dx.doi.org/10.1021/cg201447c | *Cryst. Growth Des.* 2012, 12, 975−981

Table 1. Crystal Data and Structure Refinement Parameters of Compounds 1−4

parameters	1	2	3	4
empirical formula	$C_9H_{12}CoN_2O_7$	$C_9H_{12}NiN_2O_7$	$C_{10}H_{10}CoNO_6$	$C_{10}H_{10}NiNO_6$
M	319.13	318.89	299.12	298.88
crystal stystem	orthorhombic	orthorhombic	orthorhombic	orthorhombic
space group	$P2_12_12$ (No. 18)	$P2_12_12$ (No. 18)	$P2_12_12$ (No. 18)	$P2_12_12$ (No. 18)
a (Å)	26.282(5)	26.1792(15)	27.1331(9)	26.9967(9)
b (Å)	6.620(5)	6.6400(4)	6.7002(2)	6.6856(2)
c (Å)	7.667(5)	7.6702(5)	7.6817(3)	7.6377(3)
V (Å^3)	1334.0(14)	1333.31(14)	1396.51(8)	1378.52(8)
Z	4	4	4	4
T (K)	293	293	293	293
λ (Mo K_α)	0.71073	0.71073	0.71073	0.71073
D_c (g cm^{-3})	1.564	1.564	1.413	1.430
μ (mm^{-1})	1.315	1.483	1.244	1.423
θ_{max} (deg)	25.790	25.7	25.7	25.7
total data	11386	12189	13273	17790
unique reflection	2575	2538	2659	2626
R_{int}	0.098	0.047	0.082	0.053
data [$I > 2\sigma(I)$]	1912	2072	1802	2467
R^a	0.0567	0.0458	0.0626	0.0807
$R_w{}^b$	0.1546	0.1406	0.2165	0.2599
GOF	1.065	1.22	1.12	1.31
Flack	0.02(5)	−0.02(5)	−0.05(8)	−0.05(8)

$^aR = \Sigma||F_o| - |F_c||/\Sigma|F_o|$. $^bR_w = [\Sigma\{w(F_o{}^2 - F_c{}^2)^2\}/\Sigma\{w(F_o{}^2)^2\}]^{1/2}$

the assembly of metal ions with an enantiopure organic linker renders a homochiral framework. Therefore, introduction of enantiopure linkers such as L-malate in a framework can give rise to chirality and magnetism, but to invoke porosity we can make use of a pyridyl-based long linker that can provide interaction sites as well as enough space to create voids. It is well documented that the presence of interaction sites in the pore surface enhances guest binding, making the material guest selective.[36] There is a serious interest today in environmental issues such as the increasing CO_2 concentration in the atmosphere, and MOFs are one of the promising materials to solve such problems.[37−45] We have employed two long chain linkers 4,4′-bisazobipyridine (azpy) and 1,2-bis(4-pyridyl)-ethylene (bpee) containing −N═N− (azo) −CH═CH− (ethylenic) functional groups respectively and studied the effect of such changes in functional groups on gas uptake. We have assembled mixed ligand systems (L-malate and 1,2-bis(4-pyridyl)ethylene (bpee); L-malate and 4,4′-bisazobipyridine (azpy)) with Co(II) and Ni(II) and have obtained four isostructural 3D porous frameworks with the general formulas $\{[M(L\text{-mal})(azpy)_{0.5}]\cdot 2H_2O\}$ (M = Co (**1**), Ni (**2**)) and $\{[M(L\text{-mal})(bpee)_{0.5}]\cdot H_2O\}$ (M = Co (**3**), Ni (**4**)); (L-mal = malate dianion). As the precursor itself is chiral (L-malic acid), all the four MOFs are homochiral in nature. The malate anion and the metal centers create two-dimensional (2D) magnetic sheets, and the sheets are further supported by pillars such as azpy or bpee which induce porosity and also affect the polarity inside the pore suface as realized by the highly selective CO_2 uptake.

EXPERIMENTAL SECTION

Materials. All the reagents employed were commercially available and used as provided without further purification. All the metal salts were obtained from Spectrochem, and 1,2-bis(4-pyridyl)ethylene (bpee) and L-malic acid were obtained from Sigma Aldrich chemical Co. 4,4′-Bisazobipyridine (azpy) was synthesized following a previously reported procedure.[46]

Physical Measurements. Elemental analysis was carried out using a Thermo Fischer Flash 2000 Elemental analyzer. IR spectra were recorded on a Bruker IFS 66v/S spectrophotometer using KBr pellets in the region 4000−400 cm^{-1}. Thermogravimetric analysis (TGA) was carried out (Metler Toledo) in nitrogen atmosphere (flow rate = 50 mL min^{-1}) in the temperature range 30−500 °C (heating rate = 3 °C min^{-1}). Powder X-ray diffraction (PXRD) patterns of the products were recorded by using Mo−K_α radiation (Bruker D8 Discover; 40 kV, 30 Ma). The pattern agreed with those calculated from single crystal structure determination. DC magnetic susceptibility measurements were carried out on a Vibrating Sample magnetometer, PPMS (Physical Property Measurement System, Quantum Design, USA) in the temperature range 2.5−300 K with applied field of 100 Oe. Field variation (−5 kOe to 5 kOe) magnetization measurements were carried out at 3 K. Diamagnetic corrections were applied using Pascal's constants.

Synthesis of $[\{Co(L\text{-mal})(azpy)_{0.5}\}\cdot 2H_2O]_n$ (1) and $[\{Co(L\text{-mal})(bpee)_{0.5}\}\cdot H_2O]_n$ (3). Compounds **1** and **3** were synthesized by employing solvothermal conditions at 120 °C. $Co(NO_3)_2\cdot 6H_2O$ (0.5 mmol, 0.145 g) was dissolved in 4 mL of DMF in a 20 mL glass vial; to this, an aqueous solution (2 mL) of L-malic acid (0.5 mmol, 0.067 g) was added with stirring Then ethanolic solution (2 mL) of azpy (0.25 mmol, 0.045 g) in the case of **1** or bpee (0.25 mmol, 0.041 g) in the case of **3** was added, and the mixture was stirred for 30 min to mix well. Then the vial was sealed and heated to 120 °C for 12 h. After being cooled to room temperature, beautiful orange-red crystals of **1** and red-colored crystals of **3** were isolated, washed with DMF, and dried in air. Yield (75%) for **1**. Anal. Calcd. for $C_9H_{11}CoN_2O_7$: C, 33.97; H, 3.48; N, 8.80 Found: C, 33.41; H, 3.03; N, 9.29. FT-IR (KBr pellet, 4000−400 cm^{-1}): 3475(b), 2923 (s), 2802 (w), 2645 (w), 1656 (s), 1592 (s), 1428 (s), 1301 (w), 1247 (s), 1095 (s), 836 (m), 707 (w) 619 (s), 551 (w). Yield (70%) for **3**. Anal. Calcd. for $C_{10}H_{10}CoNO_6$: C, 40.15; H, 3.37; N, 4.68. Found: C, 39.98; H, 3.03; N, 4.89. FT-IR (KBr pellet, 4000−400 cm^{-1}): 3471(b), 2921 (s), 2803 (w), 2644 (w), 1656 (s), 1599 (s), 1424 (s), 1302 (w), 1244 (s), 1091 (s), 831 (m), 705 (w) 612 (s), 555 (w).

Synthesis of $[\{Ni(L\text{-mal})(azpy)_{0.5}\}\cdot 2H_2O]_n$ (2) and $[\{Ni(L\text{-mal})(bpee)_{0.5}\}\cdot H_2O]_n$ (4). $Ni(acetate)_2\cdot 4H_2O$ (0.100 g, 0.4 mmol) and L-

dx.doi.org/10.1021/cg201447c | Cryst. Growth Des. 2012, 12, 975−981

malic acid (0.055 g, 0.4 mmol) were dissolved in 2 mL of water. To this, ethanolic solution (1 mL) of azpy (0.055 g, 0.3 mmol) in the case of **2** or bpee (0.054 g, 0.3 mmol) in the case of **4** was added. The mixture was stirred for half an hour and then taken in a 23 mL PTFE-lined acid digestion bomb and heated at 150 °C for 3 days. After being cooled to room temperature, reddish-brown crystals of **2** or light green crystals of **4** were isolated. The crystals were washed with ethanol to remove unreacted substances and dried in air. Yield (63%) for **2**. Anal. Calcd. for $C_9H_{11}NiN_2O_7$: C, 34.00; H, 3.48; N, 8.81 Found: C, 32.41; H, 4.03; N, 8.99. FT-IR (KBr pellet, 4000−400 cm^{-1}): 3477(b), 2928 (s), 2800 (w), 2643 (w), 1659 (s), 1591 (s), 1423 (s), 1305 (w), 1246 (s), 1093 (s), 836 (m), 702 (w) 615 (s), 557 (w).Yield (78%) for **4**. Anal. Calcd. for $C_{10}H_{10}NiNO_6$: C, 40.18; H, 3.37; N, 4.68. Found: C, 39.85; H, 3.03; N, 4.79. FT-IR (KBr pellet, 4000−400 cm^{-1}): 3470(b), 2926 (s), 2801 (w), 2649 (w), 1666 (s), 1598 (s), 1426 (s), 1300 (w), 1241 (s), 1092 (s), 833 (m), 701 (w) 619 (s), 557 (w).

X-ray Crystallography. X-ray single crystal structural data of **1**, **2**, **3**, and **4** were collected on a Bruker Smart-CCD diffractometer equipped with a normal focus, 2.4 kW sealed tube X-ray source with graphite monochromated Mo-Kα radiation (λ = 0.71073 Å) operating at 50 kV and 30 mA. The program SAINT[47] was used for integration of diffraction profiles and absorption correction was made with SADABS[48] program. All the structures were solved by SIR 92[49] and refined by the full matrix least-squares method using SHELXL-97.[50] All the hydrogen atoms were fixed by HFIX and placed in ideal positions. In compounds **1** and **3**, the guest water molecules are in disordered state and have been resolved in terms of occupancy. Potential solvent accessible area or void space was calculated using the PLATON multipurpose crystallographic software.[51] All crystallographic and structure refinement data of **1**, **2**, **3**, and **4** are summarized in Table 1. Selected bond lengths and angles for **1**, **2**, **3**, and **4** are given in Tables S1−S4, respectively. All calculations were carried out using PLATON and WinGX system, Ver 1.70.01.[52]

Adsorption Study. Adsorption isotherms of N_2 (77 and 195 K) CO_2, H_2, Ar, and O_2 (195 K) were recorded using the dehydrated samples of **1** (**1′**) and **3** (**3′**) by using a QUANTACHROME QUADRASORB-SI analyzer. In the sample tube, the adsorbent samples (**1′** and **3′**) (~100−150 mg) were placed which had been prepared at 190 °C under a 1 × 10^{-1} Pa vacuum for about 12 h prior to measurement of the isotherms. Helium gas (99.999% purity) at a certain pressure was introduced in the gas chamber and allowed to diffuse into the sample chamber by opening the valve. The amount of gas adsorbed was calculated from the pressure difference ($P_{cal} - P_e$), where P_{cal} is the calculated pressure with no gas adsorption and P_e is the observed equilibrium pressure. All the operations were computer-controlled and automatic.

Adsorption of H_2O at 298 K was measured in the dehydrated **1′** and **3′** in the vapor state using a BELSORP-aqua-3 analyzer. A sample of about ~100−150 mg was prepared by heating at 190 °C for about 12 h under a vacuum (1 × 10^{-1} Pa) prior to measurement of the isotherms. The solvent molecules used to generate the vapor were degassed fully by repeated evacuation. Dead volume was measured with helium gas. The adsorbate was placed into the sample tube, then the change of the pressure was monitored, and the degree of adsorption was determined by the decrease in pressure at the equilibrium state. All operations were computer controlled and automatic.

RESULTS AND DISCUSSION

Structural Description of $\{[M(L\text{-mal})(azpy)_{0.5}]\cdot 2H_2O\}_n$ (M = Co (1), Ni (2)) and $\{[M(L\text{-mal})(bpee)_{0.5}]\cdot H_2O\}_n$ (M = Co (3), Ni (4)). All four compounds (**1**−**4**) crystallize in the orthorhombic crystal system with the chiral $P2_12_12$ space group. X-ray structure determination of **1**−**4** reveals a three-dimensional (3D) framework constituted by the malate and organic pillars (azpy and bpee). Each malate dianion chelates a metal atom (Co(II) or Ni(II)) in a tridentate fashion through carboxylate and hydroxyl oxygen atoms (Figure 1), while the

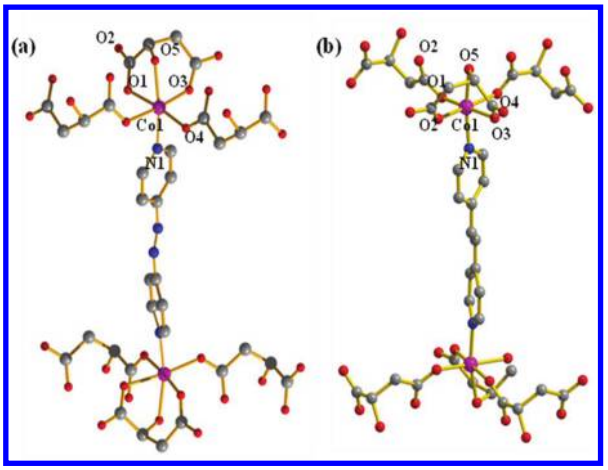

Figure 1. View of the coordination environment around Co(II) and the corresponding binding mode of malate dianion: (a) for compound **1**, (b) for compound **3**.

other two carboxylate oxygen atoms connect two other metal atoms in a syn−anti fashion resulting in a 2D corrugated sheet of $\{M(\mu_3\text{-malate})\}_n$ in the *bc* plane. Topological analysis of the 2D layer by TOPOS 4.0[51] suggests the formation of a 3-connected uninodal net with Schläfli symbol $\{6^3\}$ (Figures 2a

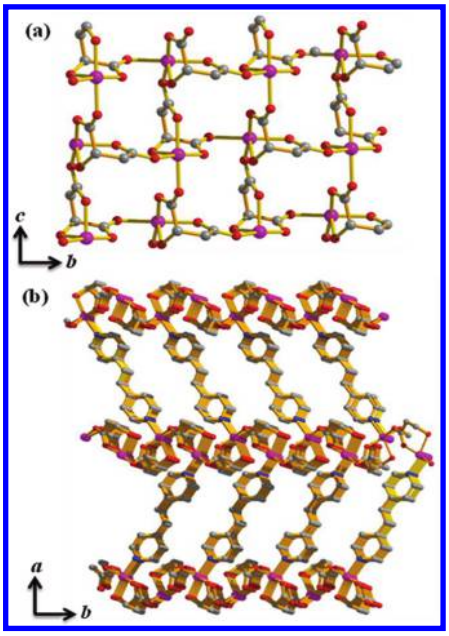

Figure 2. (a) View of the 2D sheet of $[Co\text{-}L\text{-malate}]_n$ in the crystallographic *bc* plane, (b) view of the pillared-layer 3D structure of compound **1** along the crystallographic *c*-axis.

and 3a). Each layer is further pillared by organic pyridine based linker such as azpy (for **1** and **2**) and bpee (for **3** and **4**) resulting in a 3D pillared-layer framework with one-dimensional (1D) channels occupied by guest water molecules along the crystallographic *b*-axis (Figures 2b and 4). The topology of the 3D framework suggests a (2,3,4)-connected net with Schläfli symbol $\{6^3.8^2.10\}2\{6^3\}2\{8\}$ (Figure 3b). Each framework is homochiral as observed in the respective Flack parameter (Table 1). In the 3D framework, each metal atom is in a distorted octahedral geometry with (MO_5N) chromophore which is reflected by the *cisoid* and *transoid*

dx.doi.org/10.1021/cg201447c | Cryst. Growth Des. 2012, 12, 975−981

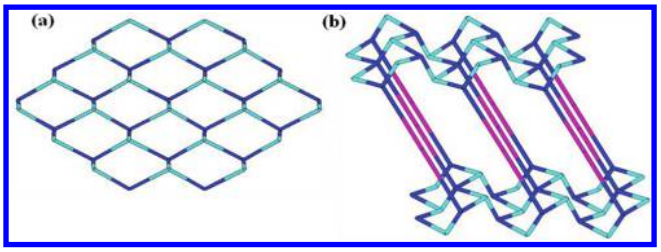

Figure 3. (a) View of the 3-connected uninodal 2D net of $[Co\text{-}L\text{-}malate]_n$ in **1** and (b) 2,3,4-connected 3D net of compound **1**.

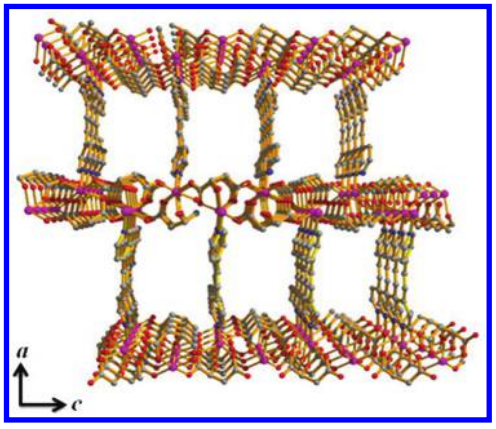

Figure 4. View of the 3D pillared-layer framework of **1** showing 1D rectangular channels along the *b* axis.

angles (Tables S1–S4, Supporting Information). In compounds **1** and **3**, the Co(II)–O bond length varies from 2.040(3)–2.193(3) Å and 2.034 (5)–2.193 (5) Å, respectively, and the corresponding Ni(II)–O bond lengths for **3** and **4** are 2.012(5)–2.137(5) Å and 2.021(4)–2.130(3) Å, respectively. Co(II)–N bond lengths in compounds **1** and **3** are 2.122(3) and 2.128(3) Å, respectively, whereas the corresponding Ni–N bond lengths in **2** is 2.085 (3) Å and in **4** is 2.089 (3) Å. In the case of **1** (or **3**), the distances between the adjacent Co(II) centers in the 2D network, Co–Co(a) connected by *α*-carboxylate and Co–Co(b) by *β*-carboxylate, are 5.351 Å (the corresponding distance for **3** is 5.391 Å) and 5.367 Å (5.398 Å for **3**), respectively. The Co···Co distance is 13.268 Å for **1** and 13.596 Å for **3** between the 2D sheets based on azpy and bpee, respectively. Such Ni···Ni distances in the case of **2** and **4** are almost similar. A rectangular-shaped channel can be viewed along the crystallographic *b* axis (Figure 4) without any significant opening along the *a*- and *c*-axis in all the cases. In compounds **1** and **2**, the dimension of the channel is ~7.0 × 6.2 $Å^2$,[53] whereas for **3** and **4** the channel size is slightly smaller, ~6.8 × 6.1 $Å^2$. The effective solvent accessible void volume of the **1** and **2** is ~29.6% (395.4 $Å^3$) per unit cell volume, and for **3** and **4** it is ~29.3% (384.1 $Å^3$).

Framework Stability. Thermogravimetric analysis (TGA) of **1** shows a weight loss of ~12% around 50–150 °C, which corresponds to the loss of two solvent water molecules (calc. wt % 11.3) (Figure S2, Supporting Information), and the dehydrated state $\{[Co(L\text{-}mal)(azpy)_{0.5}]\}_n$ (**1′**) is stable up to 240 °C. In the temperature range 240–450 °C, a ~29% weight loss was observed suggesting the loss of the azpy ligand (calc. wt % 29.5). Similarly, a weight loss of ~10% is observed up to 120 °C for **2**, which suggests the presence of two guest water molecules (Figure S3, Supporting Information), and the dehydrated framework $\{[Ni(L\text{-}mal)(azpy)_{0.5}]\}_n$ (**2′**) is stable up to 220 °C. Compound **3** shows a weight loss of ~6% around 40–150 °C corresponding to the loss of one guest solvent water molecule (calc. wt % 6.0), and this dehydrated $\{[Co(L\text{-}mal)(bpee)_{0.5}]\}_n$ (**3′**) state is stable up to 200 °C. The second weight loss of ~35% in the temperature range of 200–275 °C corresponds to the loss of the bpee linker (calc. wt % 36.0). Upon further heating, the compound decomposes to unidentified products (Figure S2, Supporting Information). For compound **4**, a weight loss of ~8% is observed suggesting the presence of one water molecule inside the pore (Figure S3, Supporting Information). PXRD patterns of the dehydrated frameworks show sharp peaks with almost similar Bragg intensities suggesting retention of the framework structures. The peak corresponding to the (200) reflection, passing through the middle of the pillars (azpy or bpee) and the guest water molecules, slightly shifted to higher angles (2θ = 6.72° to 6.96° for **1** and 6.74° to 6.97° for **3**) suggesting framework contraction upon desolvation (see Figures 5 and S4).

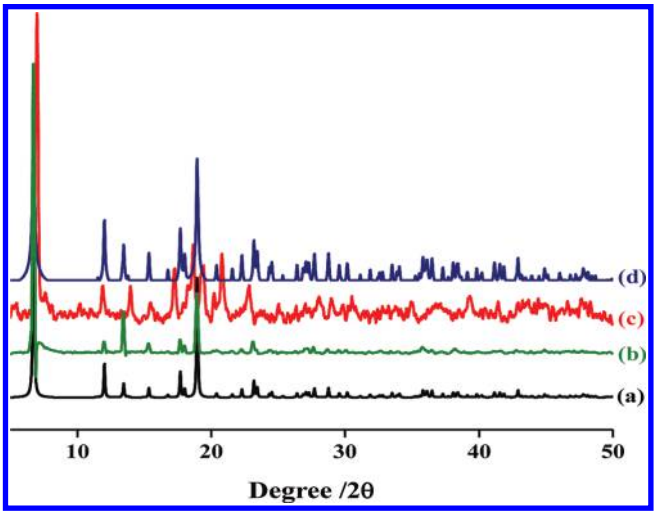

Figure 5. PXRD patterns of compound **1**: (a) simulated, (b) as-synthesized, (c) heated at 190 °C, (d) rehydrated.

Magnetic Properties. Since **1**–**4** are isostructural, the magnetic properties of only **1** and **2** are reported here. Variable temperature zero-field-cooled (ZFC) and field-cooled (FC) magnetic susceptibility data of a powder sample of **1** recorded at 100 Oe are shown in Figure 6. At 300 K, the value of $\chi_M T$ is 2.50 $cm^3\ mol^{-1}$ K with an effective magnetic moment of 4.50 μ_B per formula unit, which is higher than the spin-only value of 3.87 μ_B for a high spin Co(II) ion. The higher value of $\chi_M T$ can be attributed to the contribution from spin–orbit coupling which is commonly observed in Co(II) compounds.[54] The high temperature (75–200 K) inverse susceptibility data obeys the Curie–Weiss law with C = 2.72 $cm^3\ mol^{-1}$ K and θ = −9.7 K indicating a weak antiferromagnetic exchange interaction between the Co(II) centers. On lowering the temperature, both the FC and ZFC susceptibilities gradually increase following each other, and the value of χ_M at around 3 K is about 0.57 emu mol^{-1} at 3 K, showing no phase transition (Figure 6). The variable temperature $\chi_M T$ plot shows a continuous decrease to a minimum value of 1.74 $cm^3\ mol^{-1}$ K at 3 K (inset Figure 6). Thus, the temperature-dependent behavior of χ_M and $\chi_M T$ are in line with the antiferromagnetic behavior in **1**. The M vs H curve recorded at 3 K shows no hysteresis loop with a saturation magnetization of 1.82 μ_B per

dx.doi.org/10.1021/cg201447c | Cryst. Growth Des. 2012, 12, 975–981

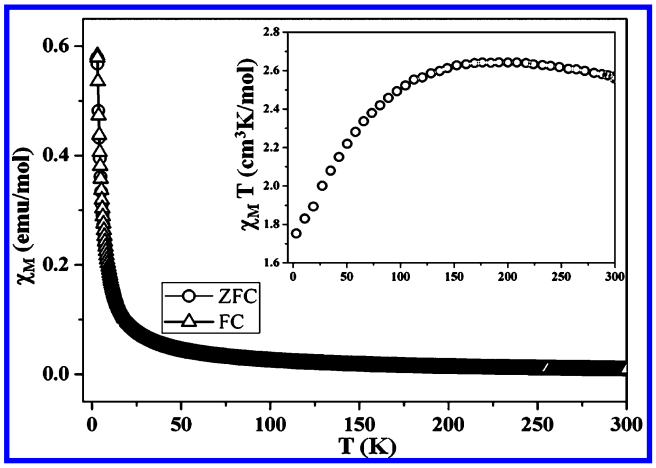

Figure 6. Temperature dependence of the magnetic susceptibility (χ_M) of **1** at 100 Oe under field-cooled (FC) and zero-field-cooled (ZFC) conditions. Inset shows temperature dependence of $\chi_M T$.

formula unit at 50 kOe which is lower than the saturation value of 3 μ_B for spin-only Co(II) ion (Figure S7, Supporting Information).[55] This behavior also supports an antiferromagnetic coupling between the Co(II) ions in **1**.

Variable-temperature ZFC and FC magnetic susceptibility data of a powder sample of **2** recorded at 100 Oe are shown in Figure 7. At 300 K, the value of $\chi_M T$ is 1.21 cm^3 mol^{-1} K with

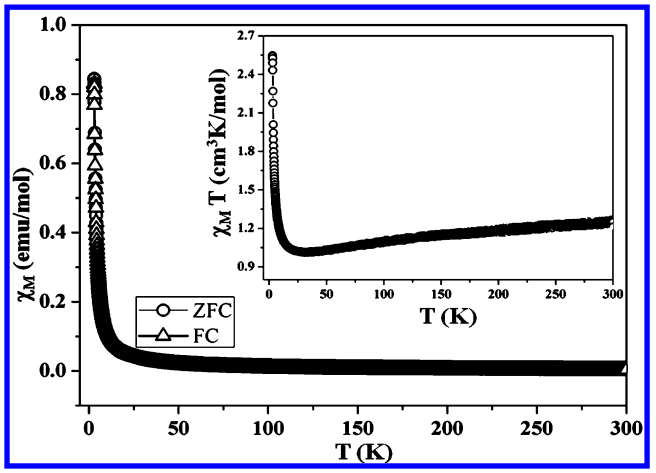

Figure 7. Temperature dependence of the magnetic susceptibility (χ_M) of **2** at 100 Oe under field-cooled (FC) and zero-field-cooled (ZFC) conditions. Inset shows temperature dependence of $\chi_M T$.

an effective magnetic moment of 3.12 μ_B per formula unit, which is slightly higher than the spin-only value of 2.83 μ_B for a Ni(II) ion. The high temperature (75−200 K) inverse susceptibility data obeys the Curie−Weiss law with C = 1.26 cm^3 mol^{-1} K and θ = −15.4 K indicating an antiferromagnetic exchange interaction between the Ni(II) centers. The low temperature FC and ZFC susceptibility data increase starting at 20 K to a maximum value of 0.84 emu mol^{-1} at 3 K showing no phase transition. The $\chi_M T$ vs T plot shows a gradual decrease of $\chi_M T$ from 300 K to a minimum value of 1.04 cm^3 mol^{-1} K at 22 K, soon after it rises to a maximum value of 2.54 cm^3 mol^{-1} K at 3 K (inset Figure 6). Thus, the high temperature susceptibility data of **2** reveal antiferromagnetic exchange coupling between the Ni(II) ions. As the temperature is lowered, ferromagnetic exchange coupling between the Ni(II) ions dominates the weak antiferromagnetic interactions observed at high temperatures. The overall magnetic behavior of **2** conforms to a ferrimagnetic type behavior. A similar magnetic behavior between the Ni(II)-malate system has been observed before.[31] The M vs H curve recorded at 3 K shows no hysteresis loop, and the observed saturation magnetization of 1.32 μ_B per formula unit at 50 kOe is lower than the saturation value of 2 μ_B for spin-only Ni(II) ions (Figure S8, Supporting Information).

Adsorption Properties. To study the porosity of these isostructural compounds, we have chosen frameworks **1** and **3** as they have different pillar linkers. Prior to measurement, both the compounds were activated by removing the guest solvent molecules at 190 °C under a vacuum. At 77 K, both the compounds show typical type II profile of N_2 (kinetic diameter, 3.64 Å)[56] adsorption isotherms suggesting only surface adsorption (Figure S9, Supporting Information), although the channel size is large enough (7.0 × 6.2 Å^2 and 6.8 × 6.1 Å^2 for compound **1** and **3** respectively) compared to the kinetic diameter of N_2. This can be attributed to the 1D channel systems running along crystallographic b axis in all the frameworks, and there are no additional effective channels along the a or c axis (Figure S10, Supporting Information). Therefore, at very low temperatures (77 K), N_2 molecules probably interact strongly with pore aperture and block other molecules to pass through, and resulting only in surface adsorption.[44] However, to our surprise CO_2 (kinetic diameter, 3.3 Å),[56] adsorption measurements at 195 K show steep uptake at low pressure regions, and a typical type I profile in both cases suggests a microporous nature of the frameworks (Figures 8

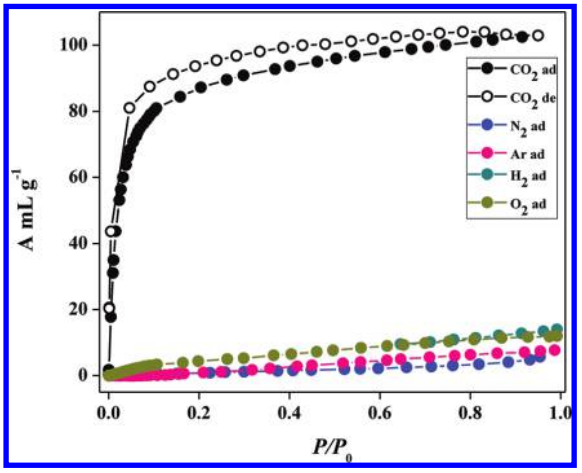

Figure 8. Adsorption studies of different gases for compound **1′**, showing a highly selective CO_2 adsorption at 195 K.

and 9). Framework **1′** exhibits ∼22 wt % uptakes, whereas framework **3′** exhibits an uptake of ∼7 wt % of CO_2. To get insight into the significant change in CO_2 uptake, we examined the pore structures of **1** and **3** carefully. As in both cases, the pore size and void space are comparable, and the layered environment is the same with an octahedral geometry of the metal ions, and it is likely that modulation in pillar linkers renders such changes in the CO_2 uptake. In compound **1**, the azpy linker contains the −N═N− group, whereas in **2**, bpee comprises the −CH═CH− group. In the host framework of **1′**, the polar azo group (−N═N−) can act as a Lewis basic site and hence it can interact with the CO_2 molecules effectively as the carbon atom in CO_2 is electron deficient (Lewis acid) in nature and provides extra energy of adsorption and higher

dx.doi.org/10.1021/cg201447c | Cryst. Growth Des. 2012, 12, 975−981

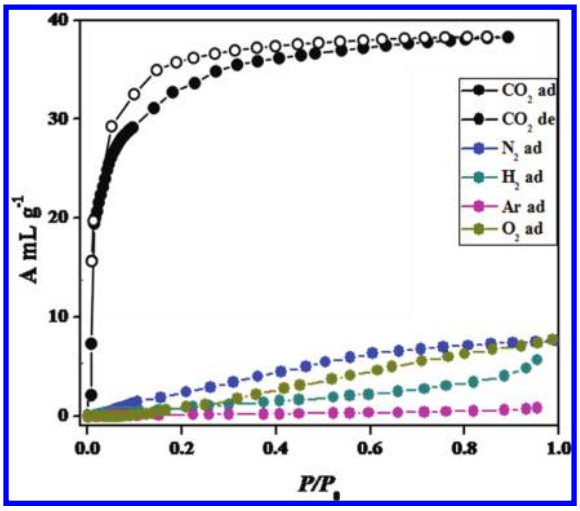

Figure 9. Adsorption studies of different gases for compound **3′**, showing highly selective CO_2 adsorption at 195 K.

uptake. Such type of interaction is not feasible in **3′**. Both profiles were analyzed by the Dubinin–Radushkevich (DR)[57] equation which imparts adsorbate–adsorbent interaction. The $q_{st\phi}$ value for **1′** and **3′** are 37 kJ mol^{-1} and 31 kJ mol^{-1}, respectively, suggesting stronger interaction of CO_2 in **1′**. The strong interaction of CO_2 with **1** would be attributed to the highly polar pore surface (decorated with −N═N− group) compared to **3** (decorated with −CH═CH−) resulting in more CO_2 uptake in **1**. To study the selectivity at 195 K, we have performed adsorption isotherm measurements of H_2 (2.83 Å), N_2, Ar (3.5 Å), and O_2 for compound **1′** and **3′**, which suggests an excellent selective nature for CO_2 at the same temperature (Figures 8 and 9).

To further investigate the polar nature of the pore surfaces, we carried out adsorption isotherm measurements of H_2O vapor (kinetic diameter, 2.65 Å).[56] Compound **1′** at 298 K shows almost a linear uptake of water vapor at low pressure, and at a relative vapor pressure $P/P_o \sim 0.65$ it rises more steeply to reach a final uptake value of ∼156 mL g^{-1} (Figure S11, Supporting Information). Compound **3′** also shows a similar adsorption profile of H_2O, and the calculation using the final uptake amount suggests that frameworks **1′** and **3′** adsorb ∼2 and ∼1.4 molecules of water per formula, respectively. In both cases, desorption curves follow a different path showing distinct hysteresis suggesting strong interaction with pore surface. The values of βE_0, which reflect the adsorbate–adsorbent affinities, are 5.16 kJ mol^{-1} and 4.47 kJ mol^{-1}, respectively, for **1′** and **3**, suggesting greater polarity of the pore surface in **1** compared to **3′**.

CONCLUSIONS

In conclusion, we have successfully synthesized four chiral isostructural porous 3D frameworks of Co(II) and Ni(II), $\{[M(L\text{-mal})(azpy)_{0.5}]\cdot 2H_2O\}_n$ (M = Co (**1**), Ni (**2**)) and $\{[M(L\text{-mal})(bpee)_{0.5}]\cdot H_2O\}_n$ (M = Co (**3**), Ni (**4**)), using a mixed ligand system with L-malate as the chiral precursor. On the basis of a suitable choice of different building units (metal ions) and organic linkers, it has been possible to attain chirality, porosity, and magnetic properties in the same material. The present study demonstrates how pillar modulation in the frameworks affects the polarity of the pore surface which determines the selectivity and magnitude of CO_2 uptake.

ASSOCIATED CONTENT

Supporting Information

Table of bond lengths and angles for **1**–**4**; FTIR spectra for **1**–**4**; thermogravimetric analysis for **1**–**4**; PXRD for **2**–**4**; *M* vs *H* curve for **1** and **2**; nitrogen adsorption–desorption isotherm for **1′** and **3′**; spacefilled view of **1** along different crystallographic axes; H_2 adsorption–desorption profile of compound **1′**; H_2O vapor adsorption–desorption isotherms of compounds **1′** and **3′**; crystallographic information file. This material is available free of charge via the Internet at http://pubs.acs.org.

AUTHOR INFORMATION

Corresponding Author

*E-mail: tmaji@jncasr.ac.in (T.K.M.); cnrrao@jncasr.ac.in (C.N.R.R.); fax: 91-80 22082766.

ACKNOWLEDGMENTS

We thank Dr. A. Sundaresan for magnetic measurements and C.M.N. thanks DRDO, India, for a fellowship. T.K.M. gratefully acknowledges the financial support from DST, Govt. of India (Fast Track Proposal). R.H. acknowledges DST, JNCASR, India.

REFERENCES

(1) Moulton, B.; Zaworotko, M. J. *Chem. Rev.* **2001**, *101*, 1629.
(2) Yaghi, O. M.; O'Keeffe, M.; Ockwig, N. W.; Chae, H. K.; Eddaoudi, M.; Kim, J. *Nature* **2003**, *423*, 705.
(3) Rao, C. N. R.; Natarajan, S.; Vaidhyanathan, R. *Angew Chem., Int. Ed.* **2004**, *43*, 1466.
(4) Kitagawa, S.; Kitaura, R.; Noro, S. *Angew Chem., Int. Ed.* **2004**, *43*, 2334.
(5) Zukal, A.; Dominguez, I.; Mayerová, J.; Cezka, J. *Langmuir* **2009**, *25*, 10314.
(6) Siriwardane, R. V.; Shen, M. S.; Fisher, E. P.; Losch, J. *Energy Fuels* **2005**, *19*, 1153.
(7) Kim, S. N.; Son, W. J.; Choi, J. S.; Ahn, W. S. *Microporous Mesoporous Mater.* **2008**, *116*, 394.
(8) Lee, J. Y.; Farha, O. K.; Roberts, J.; Sheidt, K. A.; Nguyen, S. B. T.; Hupp, J. T. *Chem. Soc. Rev.* **2009**, *38*, 1450.
(9) Horike, S.; Dinca, M.; Tamaki, K.; Long, J. R. *J. Am. Chem. Soc.* **2008**, *130*, 5854.
(10) Dybtsev, D. N.; Nuzhdin, A. L.; Chun, H.; Bryliakov, K. P.; Talsi, E. P.; Fedin, V. P.; Kim, K. *Angew Chem., Int. Ed.* **2006**, *45*, 916.
(11) Hasegawa, S.; Horike, S.; Matsuda, R.; Furukawa, S.; Mochizuki, K.; Kinoshita, Y.; Kitagawa, S. *J. Am. Chem. Soc.* **2007**, *129*, 2607.
(12) Chae, H. K.; Eddaoudi, M.; Kim, J.; Hauck, S. I.; Hartwig, J. F.; O'Keeffe, M.; Yaghi, O. M. *J. Am. Chem. Soc.* **2001**, *123*, 11482.
(13) Eddaoudi, M.; Moler, D. B.; Li, H. L.; Chen, B. L.; Reineke, T. M.; O'Keeffe, M.; Yaghi, O. M. *Acc. Chem. Res.* **2001**, *34*, 319.
(14) Pan, L.; Parker, B.; Huang, X.; Olson, D. H.; Lee, J. Y.; Li, J. J. *J. Am. Chem. Soc.* **2006**, *128*, 4180.
(15) Kanoo, P.; Gurunatha, K. L.; Maji, T. K. *J. Mater. Chem.* **2010**, *20*, 1322.
(16) Horcazada, P.; Serre, C.; Sebban, M.; Taulelle, F.; Férey, G. *Angew Chem., Int. Ed.* **2006**, *45*, 5974.
(17) Horcazada, P.; Serre, C.; Maurin, G.; Ramsahye, N. A.; Balas, F.; Vallet-Regi, M.; Sebban, M.; Taulelle, F.; Férey, G. *J. Am. Chem. Soc.* **2008**, *130*, 6774.
(18) Ke, F.; Yuan, Y.-P.; Qiu, L.-G.; Shen, Y. H.; Xie, A.-J.; Zhu, J.-F.; Tian, X.-Y.; Zhang, L.-D. *J. Mater. Chem.* **2011**, *21*, 3843.
(19) Hazra, A.; Kanoo, P.; Maji, T. K. *Chem. Commun.* **2011**, *47*, 538.
(20) Kurmoo, M. *Chem. Soc. Rev.* **2009**, *38*, 1353.
(21) Konar, S.; Mukherjee, P. S.; Zangrando, E.; Lloret, F.; Chaudhuri, N. R. *Angew Chem., Int. Ed.* **2002**, *41*, 1561.
(22) Liu, T. F.; Sun, H. L.; Gao, S.; Zhang, S. W.; Lau, T. C. *Inorg. Chem.* **2003**, *42*, 4792.

(23) Maji, T. K.; Sain, S.; Mostafa, G.; Lu, T. H.; Ribas, J.; Montfort, M.; Chaudhury, N. R. *Inorg. Chem.* **2003**, *42*, 709.
(24) Ma, C. B.; Chen, C. N.; Liu, Q. T.; Chen, F.; Liao, D. Z.; Li, L. C.; Sun, L. C. *Eur. J. Inorg. Chem.* **2003**, 2872.
(25) Guillou, N.; Pastre, S.; Livage, C.; Férey, G. *Chem. Commun.* **2002**, 2358.
(26) Lee, E. W.; Kim, Y. J.; Jung, D. Y. *Inorg. Chem.* **2002**, *41*, 501.
(27) Karipides, A. *Inorg. Chem.* **1979**, *18*, 44.
(28) Zhou, Z. Z.; Wang, G. F.; Hou, S. Y.; Wan, H. L.; Tsai, K. R. *Inorg. Chim. Acta* **2001**, *314*, 184.
(29) Biagioli, M.; Strinna-Erre, L.; Micera, G.; Panzanelli, A.; Zema, M. *Inorg. Chim. Acta* **2000**, *310*, 1.
(30) Kaliva, M.; Giannadaki, T.; Salifoglou, A. *Inorg. Chem.* **2001**, *40*, 3711.
(31) Duan, L.-M.; Xie, F.-T.; Chen, X.-Y.; Chen, Y.; Lu, Y.-K.; Cheng, P.; Xu, J.-Q. *Cryst. Growth Des.* **2006**, *6*, 1101.
(32) Dja, A.; Rabu, P.; Rogez, G.; Welter, R. *Chem.—Eur. J.* **2006**, *12*, 7627.
(33) Zeng, M.-H.; Feng, X.-L.; Zhang, W.-X.; Chen, X.-M. *Dalton Trans.* **2006**, *35*, 5294.
(34) Xie, F.-T.; Duan, L.-M.; Xu, J.-Q.; Ye, L.; Liu, Y.-B.; Hu, X.-X.; Song, J.-F. *Eur. J. Inorg. Chem.* **2004**, 4375.
(35) Ghosh, A.; Rao, C. N. R. *Z. Anorg. Allg. Chem.* **2008**, *634*, 1115.
(36) Vaidhyanathan, R.; Iremonger, S. S.; Dawson, K. W.; Shimizu, G. K. H. *Chem. Commun.* **2009**, *35*, 5230.
(37) D'Alessandro, D. M.; Smit, B.; Long., J. R. *Angew Chem., Int. Ed.* **2010**, *49*, 2.
(38) Mulfort, K. L.; Farha, O. K.; Malliakas, C. D.; Kanatzidis, M. G.; Hupp, J. T. *Chem.—Eur. J.* **2010**, *16*, 276.
(39) Caskey, S. R.; Wong-Foy, A. G.; Matzger., A. J. *J. Am. Chem. Soc.* **2008**, *130*, 10870.
(40) Dietzel, P. D. C.; Besikiotis, V.; Blom, R. *J. Mater. Chem.* **2009**, *19*, 7362.
(41) Samsonenko, D. G.; Kim, H.; Sun, Y.; Kim, G.-H.; Lee, H.-S.; Kim, K. *Chem.—Asian. J.* **2007**, *2*, 484.
(42) Wang, B.; Côté, A. P.; Furukawa, H.; O'Keeffe, M.; Yaghi., O. M. *Nature* **2008**, *453*, 207.
(43) Maji, T. K.; Matsuda, R.; Kitagawa., S. *Nat. Mater.* **2007**, *6*, 142.
(44) Kanoo, P.; Haldar, R.; Cyriac, S. T.; Maji, T. K. *Chem. Commun.* **2011**, *47*, 11038.
(45) Dey, R.; Haldar., R.; Maji, T. K.; Ghoshal, D. *Cryst. Growth. Des.* **2011**, *11*, 3905.
(46) Brown, E. V.; Granneman, G. R. *J. Am. Chem. Soc.* **1975**, *97*, 62.
(47) *SMART (V 5.628), SAINT (V 6.45a), XPREP, SHELXTL*; Bruker AXS Inc.: Madison, Wisconsin, USA, 2004.
(48) Sheldrick, G. M. *Siemens Area Detector Absorption Correction Program*; University of Götingen, Götingen, Germany, 1994.
(49) Altomare, A.; Cascarano, G.; Giacovazzo, C.; Gualaradi, A. *J. Appl. Crystallogr.* **1993**, *26*, 343.
(50) Sheldrick, G. M. *SHELXL-97, Program for Crystal Structure Solution and Refinement*; University of Götingen: Götingen, Germany, 1997.
(51) Spek, A. L. *J. Appl. Crystallogr.* **2003**, *36*, 7.
(52) Farrugia, L. J. WinGX-A Windows Program for Crystal Structure Analysis. *J. Appl. Crystallogr.* **1999**, *32*, 837.
(53) The sizes of the channels were calculated considering the van der Waals radii of the atoms.
(54) Nagaraja, C. M.; Kumar, N.; Maji, T. K.; Rao, C. N. R. *Eur. J. Inorg. Chem.* **2011**, 2057.
(55) Wang, X.-Y.; Gan, L.; Zhang, S.-W.; Gao, S. *Inorg. Chem.* **2004**, *43*, 4615.
(56) Webster, C. E.; Drago, R. S.; Zerner, M. C. *J. Am. Chem. Soc.* **1998**, *120*, 5509.
(57) Dubinin, M. M. *Chem. Rev.* **1960**, *60*, 235.